IET Electric Power Applications

Research Article

IET Journals
The Institution of Engineering and Technology

Design methodologies for the output power maximisation of synchronous reluctance machines

ISSN 1751-8660
Received on 5th November 2018
Revised 23rd March 2019
Accepted on 26th March 2019
E-First on 17th May 2019
doi: 10.1049/iet-epa.2018.5801
www.ietdl.org

Marco Palmieri[1] ✉, *Giuseppe Leonardo Cascella*[1], *Francesco Cupertino*[1]

[1]*Department of Electrical Engineering and Information Technology, Politecnico di Bari, via E. Orabona, 4, Bari, Italy*

✉ *E-mail: marco.palmieri@poliba.it*

Abstract: Synchronous reluctance (SyR) machines can constitute a promising alternative to permanent magnet machines for low-cost applications. The recent literature reports some guidelines for choosing the proper number and position of the rotor flux barriers capable of enhancing the electromagnetic performance in low-speed applications. However, as the rotational speed increases, the electromagnetic and structural mutual interactions become relevant; therefore, an optimal design requires a proper trade-off between torque production and stress reduction, which can be difficultly predicted analytically. This work proposes an approach based on optimisation algorithms in order to find 'non-conventional' geometries able to improve the power density: genetic algorithms coupled to magneto-static finite elements analysis and structural analytical models, are adopted to co-design SyR machines with different numbers of stator slots and rotor barriers subjected to the same thermal constraints. This study investigates two design procedures aimed at maximising the output power of SyR machines by increasing the rotational speed. Both procedures allow determining the power limits for a given volume of active parts and a fixed amount of admissible losses; moreover, the second procedure automatically finds also the rotational speed which maximises the output power.

Nomenclature

B	flux density
γ	current vector angle (dq-reference frame)
D	stator outer diameter
$\Delta\alpha_i$	position at the air gap (ith flux barrier)
F	force
f	electrical frequency
h_{ci}	thickness (ith flux barrier)
K_j	specific loss index
L	axial length of the machine
M	mass
P_{Fe}	iron losses
p.u.	per unit
r_{Gi}	centre of gravity of the ith rotor region
ρ	mass density
Σ_i	area of the ith rotor region
T_{AV}	average torque
ΔT	torque ripple
w_{rj}	width of the jth radial rib
ω	rotational speed

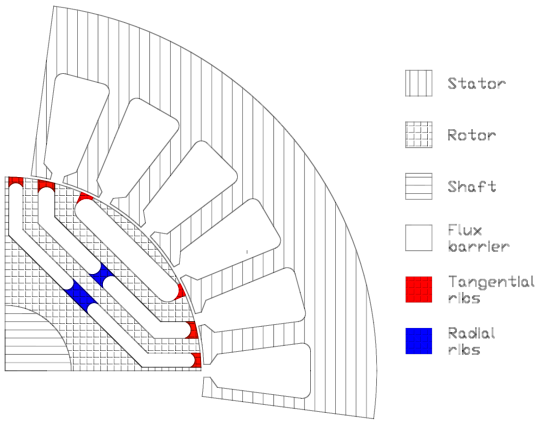

Fig. 1 *Sketch of one pole of a SyR machine*

1 Introduction

Synchronous Reluctance (SyR) machines have been receiving a renewed interest from both industry and academia in the last few years [1]. Their fields of application and power sizes are rather wide, ranging from few kilowatt devices for the more electric transportation [2] to high power generation systems [3]. The torque production of SyR machines relies on the magnetic anisotropy of the rotor structure, which is usually produced by introducing non-magnetic regions (namely the flux barriers) inside the rotor lamination, as shown in Fig. 1. Due to their passive rotor, SyR machines present several advantages with respect to other topologies: firstly, the absence of permanent magnets (PMs) implies no risks of demagnetisation, no uncontrolled voltages in case of faults and good field weakening capability; furthermore, the costs for the active parts can be definitely reduced. Moreover, the absence of windings on the rotor guarantees higher efficiencies compared to similar-sized induction motors [4]. Finally, thanks to the passive rotor, the great part of the total loss is concentrated in the stator core and windings, therefore the heat extraction results easier and the cooling system can be simplified [2].

SyR machines can be a viable alternative to PM machines and induction motors also for high-speed applications [2, 5]. Differently from surface-mounted PM synchronous machines (SPMSMs), SyR ones do not require retaining sleeves because the rotor structure itself guarantees the mechanical integrity against centrifugal forces at high speed; this can constitute a further advantage with respect to the limitation of the rotor loss but, at the same time, it requires a careful sizing of the tangential and radial ribs (see Fig. 1). The width of the rotor ribs, in fact, affects both mechanical and electromagnetic performance: thicker ribs enhance the former but worsen the latter with particular reference to average torque and power factor.

In the literature, different papers deal with the design of SyR machines: generally, analytical methods are attractive because they reduce the computational burden and allow a quick sizing of the machine; nevertheless, finite element analysis (FEA) is essential, at least in the final design stage, in order to accurately evaluate the overall performance. An analytical design approach aimed at minimising the torque ripple is reported in [6], where the authors

propose a simple criterion for choosing the number of stator slots and rotor barriers valid if the rotor equivalent slots are equally spaced around the periphery. In [7], the rule for the torque ripple minimisation based on the constant rotor slot pitch concept is adapted to SyR rotors with unsymmetrical structures through the introduction of an imaginary rotor slot opening located near the outer flux guide. Recently, also in [5], some analytical procedures are proposed for preliminary electromagnetic sizing of SyR machines: the flux barriers geometry and positions are quickly evaluated with the aim of minimising the torque ripple; however, the saturation of the ferromagnetic material, the stator slotting and the iron ribs are neglected. In [8], an improved reluctance network is adopted in order to account for the non-linear behaviour of the rotor materials, especially in the highly saturated regions.

The design issues of SyR machines are often addressed by means of optimisation algorithms coupled with FEA [9–13]. An automated procedure for the design of SyR machines based on FEA and multi-objective optimisation algorithms is proposed in [11]: a simple parameterisation of the rotor flux barriers is adopted and the electromagnetic torque is evaluated considering few magneto-static FEA simulations in order to reduce the computational burden; the quantities simultaneously optimised are the average torque and the torque ripple. A similar approach is implemented in [12] considering a more complex shape of the flux barriers and various combinations of stator slots and rotor barriers in order to point out their influence on the torque capability and iron losses of SyR machines. However, in [11, 12], only the rotor structure is optimised and the analysis is limited to low rotational speed values, which allow neglecting the mechanical issues due to the structural ribs and their influence on the electromagnetic performance. A particularly complex rotor parameterisation, comprising up to 37 variables, is adopted in [13], in order to optimise the torque and the torque ripple of SyR machines with asymmetrical flux barriers with different tip shapes; however, this latter procedure is highly time-consuming due to the huge computational burden.

All the cited works assume that the flux barriers shape is pre-determined before starting the optimisation. A different approach is proposed in [14], where the rotor geometry is constrained simply by the shaft and the air gap radii, while the space in between is partitioned into a grid of sub-regions which may contain air or iron; therefore, the task of the optimisation algorithm is to determine the materials distribution which minimises the selected design objectives. This approach, even if removes the constraints typical of the traditional designs, has a heavy computational burden; moreover, it can be barely adapted to the automatic magnetic and mechanical co-design of high-speed machines.

In order to address both mechanical and electromagnetic issues related to the design of high-speed machines, an extension of the automated design procedure presented in [11] is proposed in [15, 16]: the first work refers to SPMSMs with retaining sleeve, the latter to SyR machines. In both works, optimisation algorithms are coupled to the electromagnetic FEA plus analytical structural model for the sizing of the retaining sleeve or the structural ribs, respectively. However, the analysis in [16] is limited to a fixed number of stator slots and rotor barriers; moreover, the geometrical parameters varied by the optimisation algorithm regard the rotor lamination only.

In this study, the procedures presented in [11, 12, 16] are extended to SyR machines designed for high-speed applications; moreover, different combinations of stator slots and rotor barriers are investigated. Furthermore, a full optimisation of stator and rotor is performed.

The work has a two-fold scope: first, to address the influence of the stator slots and rotor barriers combinations on the power density maximisation of SyR machines; secondly, to find the value of rotational speed which guarantees the maximum output power for a given value of overall volume and total losses, for each combination of slots and barriers. Two automated design procedures, based on two-objective optimisations coupled to fast magneto-static FEA plus an analytical structural model for the sizing of the rotor structural ribs, are presented and compared. As will be highlighted in the subsequent sections, the first procedure is composed of two consecutive steps: at first the machine geometry is automatically designed so to optimise the average torque and the torque ripple at low speed; then the thickness of the structural ribs is designed so to withstand higher speeds and maximise the power density for a given amount of total loss; then it designs the thickness of the structural ribs so as to withstand higher speeds and maximise the power density for a given amount of total loss. The second procedure optimises the output power and the torque ripple; the rotational speed is included among the optimisation parameters in order to automatically find the speed, which maximises the output power together with the stator/rotor geometrical parameters.

The remainder of the paper is organised as follows: the problem statement, the machine parameterisation, and the optimisation settings are reported in Section 2. The two procedures proposed for the design of SyR machines are described in Sections 3 and 4, respectively, whereas their comparison is performed in Section 5. After that, in Section 6, one machine is selected and accurately analysed through both magnetic and structural FEA. Finally, the main conclusions are drawn in Section 7.

2 Problem statement

With the aim of maximising the output power, several SyR machines are designed through multi-objective optimisations: a finite element model is adopted in order to analyse the electromagnetic aspects, while an analytical model accounts for the structural ones. The design is performed starting from the open-source tool SyR-e [17]. Two values of stator slot numbers (24 and 36 slots) and three values of rotor barriers per pole (2, 3, 4 barriers), for a total of six combinations, are investigated.

All the machines share the geometrical quantities listed in Table 1. The outer diameter, the shaft radius, and the axial length are fixed, as well as the air gap thickness. The number of poles is limited to four, so to reduce iron losses. Moreover, an integer-slot single layer winding is considered in order to maximise the fundamental winding factor and the torque. The same amount of total loss (copper loss plus iron loss) is imposed for all the machines; for this purpose, index K_j, presented in [16], is considered

$$K_j = \frac{P_{\text{Loss}}}{\pi \cdot D \cdot L}, \tag{1}$$

where P_{LOSS} represents the total loss, D and L are the outer diameter and the axial length of the stator core, respectively. Here it is assumed that the machines are liquid-cooled and that all the heat is exchanged through the outer surface of the stator core, thus a K_j equal to 30 kW/m^2 is imposed. Considering the outer dimensions reported in Table 1, the admissible losses amount to 1 kW.

Dealing with high-speed applications, the selection of the magnetic materials plays an essential role: regarding the rotor, the key factors to account for are the yield strength and the specific losses [16]. On this basis, the silicon–iron alloy 10JNEX900 [18] is adopted for both stator and rotor. This material is produced by the JFE Steel Corporation with a lamination thickness equal to 0.1 mm; its yield strength is 605 MPa whereas its specific losses P_{Fe}, as a function of the frequency f and flux density B, are described by (2)

$$P_{\text{Fe}} = [5720 \cdot f^{1.16} \cdot B^{1.79} + 3.71 \cdot (fB)^2] \cdot 10^{-6} \tag{2}$$

2.1 Machine parameterisation

The stator and rotor laminations of the SyR machines are drawn automatically by the proposed design tool. For this purpose, a simple but effective geometry parameterisation of the complete machine is adopted; the stator core is defined by three parameters: the tooth length, the tooth width, and the inner diameter, independently from the chosen number of slots; moreover, all the stator teeth have a constant width. Conversely, the rotor parameters adjusted during the optimisation are two per barrier, namely the

Table 1 Common parameters shared by all the machines

Parameter	Value
stator outer diameter	90 mm
axial length	120 mm
number of poles	4
air gap length	0.35 mm
shaft diameter	10 mm
admissible loss	1 kW

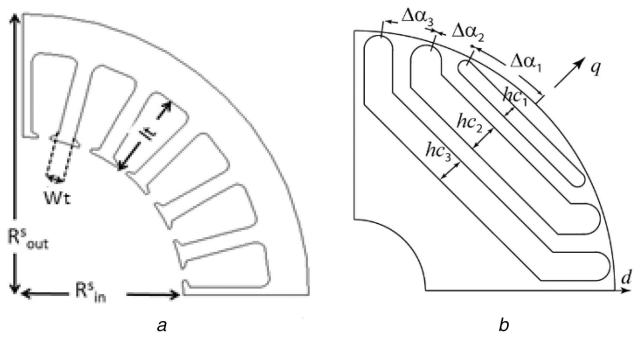

Fig. 2 *Machine parameterization*
(a) Stator, ***(b)*** Rotor

Table 2 Geometrical parameters varied during the optimisation and limits of the search space

Parameter	Lower bound	Upper bound
stator tooth length, mm	10	20
stator tooth width, mm	1.5	5
stator inner radius, mm	18	30
rotor *i*th barrier angle at the air gap, p.u.	0.1	1
rotor *i*th barrier thickness, p.u.	0.2	1

thickness and the angular position at the air gap of each barrier. The rotor barriers have a constant thickness and are simply described by straight segments; the barriers' tips are constituted by two arcs joined together in one point, which defines the angular position of the barrier at the air gap. Even though asymmetric flux barriers, as well as more complex shapes of the barriers' tips, could reduce the torque ripple more effectively [13], their optimal design would require a more complex parameterisation; therefore, in this work, flux barriers symmetrical with respect to the *d*-axis and *q*-axis are considered so to simplify the rotor construction and reduce the computational burden. For the same reasons, neither the stators nor the rotors are skewed.

All the geometrical quantities varied by the optimisation algorithm during the design are shown in Fig. 2, while Table 2 reports the limits of the search space. The rotor parameters are expressed in p.u., considering the total angle and thickness available for all the barriers as base values. Therefore, the geometry of each candidate machine is described by a vector of $2n_{\text{lay}} + 3$ elements, being n_{lay} the number of barriers per pole.

2.2 Optimisation settings

The differential evolution (DE) algorithm [19] is selected among the meta-heuristic optimisation algorithms because its effectiveness for problems related to the design of electrical machines was already proven in the literature [12, 15, 20].

During the optimisation, the DE algorithm iteratively modifies a set of candidate machines (individuals), which evolve for a given number of generations, according to some probabilistic rules. The goal of the optimisation algorithm is to find a global minimum of the chosen cost functions. In this work, the number of cost functions to be simultaneously optimised is limited to two, so to reduce the computational burden. Moreover, the candidate machines are sorted considering the 'dominance' criterion [19]: the set of the non-dominated solutions constitutes the Pareto front in the selected objectives plane. Since all the Pareto optimal machines are equally good with respect to the two-objective problem, the final choice lies with the designer.

The number of parameters describing each machine is related to the number of barriers per pole, as reported in Section 2.1. In order to fairly compare the various slots/barriers combinations, the number of individuals and generations is adapted to the number of parameters to be optimised (then it changes with the number of barriers per pole): each optimisation run is performed considering a number of individuals equal to ten times the size of the vector describing each machine, iterated for a number of generations equal to 1.2 times the number of individuals as suggested in [15]. The crossover rate is fixed at 0.95, while the mutation factor is randomly selected in the range [0, 1.5] for all the optimisation runs.

2.3 Sizing of the structural ribs

Since no retaining sleeve is adopted, the rotor integrity against the centrifugal forces must be guaranteed by the tangential and radial ribs. The thickness of the rotor ribs affects both magnetic and mechanical performance; the former worsens with the width of the total rib per barrier (with no distinction between tangential or radial ones); the latter improves with the ribs' thickness, but the radial ribs play the key role in the stress reduction [21]. Starting from these considerations, the thickness of the tangential ribs is kept fixed to the minimum manufacturing width, whereas that of the radial ribs is adapted to the mechanical speed.

A quick sizing of the radial ribs is automatically performed considering the analytical model described in [16]: as reported in Fig. 3, a single radial rib in the middle of each barrier is considered and its thickness is evaluated assuming that the *j*th rib has to withstand the centrifugal force F_j due to the whole iron region located between the rib and the rotor circumference (green area in Fig. 3). The width w_{rj} of the *j*th radial rib is computed by (3)–(5)

$$M_j = \rho \cdot L \cdot \Sigma_j, \tag{3}$$

$$F_j = M_j \cdot r_{G_j} \cdot \omega_{\max}^2, \tag{4}$$

$$w_{rj} = \frac{F_j}{L \cdot K \cdot \sigma_{\max}}, \tag{5}$$

where M_j, r_{Gj} and Σ_j are the mass, centre of gravity and surface of the jth iron region connected to the j-th radial rib (green area in Fig. 3), F_j is the centrifugal force, ρ and $\sigma_{\max}$ are the material density and yield strength, ω is the rotational speed and K is a safety factor.

This procedure gives a conservative estimation of the rib thickness. As evidenced in [21], the single radial rib can be split into two or more parts and rotated in order to relax the maximum stress; this modification does not affect the electromagnetic performance if the total width of the ribs per each barrier is kept constant.

3 Average torque–torque ripple optimisation

The first design procedure is based on the optimisation of the average torque and the torque ripple for each combination of stator slots and rotor flux barriers (T–ΔT optimisation). The former is computed as the mean value over one electrical period of the electromagnetic torque, FEA evaluated considering five rotor positions (equally spaced over one slot pitch) and a random offset [11]; the latter is calculated as the ratio between the standard deviation of the electromagnetic torque T over one electrical period and the average torque $T_{\rm AV}$, as in (6)

$$\Delta T_{\%} = \frac{\text{std}(T)}{T_{\rm AV}} \times 100. \tag{6}$$

During the optimisation, besides the geometrical quantities describing each machine reported in Section 2, also the phase angle of the current vector in the dq-reference frame is introduced as a further optimisation parameter [11]. This allows to automatically finding the MTPA trajectory very quickly, without performing several FEA simulations.

The machines are firstly designed considering a low value of the mechanical speed equal to 1000 rpm. Due to the low speed value, the iron losses in the stator and rotor cores are neglected, thus the total amount of losses is supposed to be concentrated in the stator windings. For the same reason, no radial ribs are considered because the rotor integrity is fully guaranteed by the tangential ribs, whose width is set to the minimum manufacturing thickness.

Once the optimal values for the stator and rotor geometrical parameters are found by the genetic algorithm, one machine is chosen from the Pareto front in the $T_{\rm AV}$–ΔT plane. Then, the speed is manually increased by discrete steps and the torque is FEA-evaluated for each speed value. At this stage, all the geometric parameters are kept unchanged; only the radial ribs thicknesses are adapted according to the actual speed and the current is reduced so as to maintain a constant sum of copper and iron losses.

The key performance figures of the six optimal machines selected after the T–ΔT optimisation performed at low speed (1000 rpm) are collected in Table 3. Besides the average torque and the torque ripple, which are the quantities directly optimised, the power factor and the saliency ratio (defined as the ratio between the d-axis inductance and the q-axis inductance) are reported. It can be noted that machines with high saliency ratios show high values of average torque and power factor; nevertheless, the latter remains quite low with respect to PM machines.

Finally, Table 3 shows the split ratio and magnetic insulation ratio along the q-axis of the six machines. The first one is the ratio between the inner and the outer stator diameters; the second one is the ratio between the thicknesses of air and iron of the rotor core along the q-axis. The value of the split ratio, which maximises the torque, is similar for all the slots/barriers combinations. The optimal magnetic insulation ratio varies between 0.3 and 0.37.

It can be noted that the 36 slots/4 barriers per pole combination shows superior performance in terms of torque capability, whereas

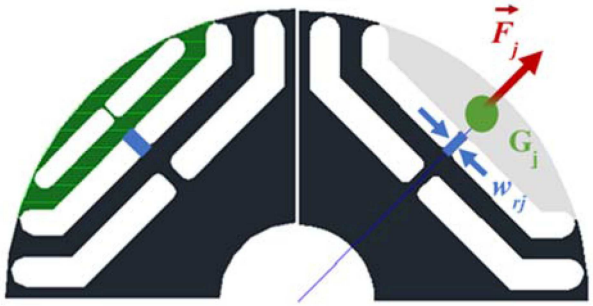

Fig. 3 *Analytical evaluation of the jth radial rib thickness*

Table 3 Main performance figures of the optimal machines at 1000 rpm (T–ΔT optimisation at low speed)

Machine	Average torque, Nm	Torque ripple, Nm	Power factor	Saliency ratio (L_d/L_q)	Split ratio, %	Air to iron ratio, %
24 slots/2 barriers per pole	11.2	2.0	0.61	3.3	55	35
24 slots/3 barriers per pole	12.5	1.6	0.67	4.0	55	35
24 slots/4 barriers per pole	12.5	1.7	0.66	4.0	55	36
36 slots/2 barriers per pole	12.5	1.0	0.67	4.0	56	30
36 slots/3 barriers per pole	12.6	1.7	0.65	3.8	52	37
36 slots/4 barriers per pole	12.9	1.0	0.67	4.1	54	33

the 24 slots/2 barriers per pole is a poor choice; the remaining slots/barriers combinations perform similar to each other. These results are consistent with those presented in the literature: in fact, at low speed, high values of stator slots and rotor barriers are beneficial to the torque capability and to the torque ripple reduction for SyR machines [12, 22].

The stator and rotor laminations of the six machines, selected after the T–ΔT optimisations, are shown in Fig. 4: among them, some machines present flux barriers disposed so as to produce a 'regular' rotor slot pitch, consistent with the guidelines reported in [6] for the torque ripple minimisation; these 'conventional' arrangements of the flux barriers can be considered the state-of-the-art solutions for the torque ripple reduction of SyR machines with symmetric barriers. Nevertheless, it is worth noticing that for few slots/barriers' combinations (e.g. the machine with 36 slots/4 barriers per pole) the DE algorithm was able to find an 'unconventional' arrangement of the flux barriers which is more effective in terms of torque ripple reduction.

Starting from the six machines shown in Fig. 4, the mechanical speed ω is increased up to 75,000 rpm without changing the stator and rotor geometric parameters found by the optimisation algorithm; the thickness of the radial ribs is automatically adapted to the considered rotational speed according to the simplified model presented in Section 2.3. The machines obtained are finally analysed by means of transient with motion electromagnetic FEA, considering a fixed amount of specific losses ($K_j = 30$ kW/m^2) for each value of the mechanical speed: for this purpose, copper, and iron losses are FEA-evaluated through the software MagNet by Infologic Design; moreover, the current amplitude and phase angle are manually adapted for each mechanical speed so to work on the maximum torque per ampere (MTPA) trajectory.

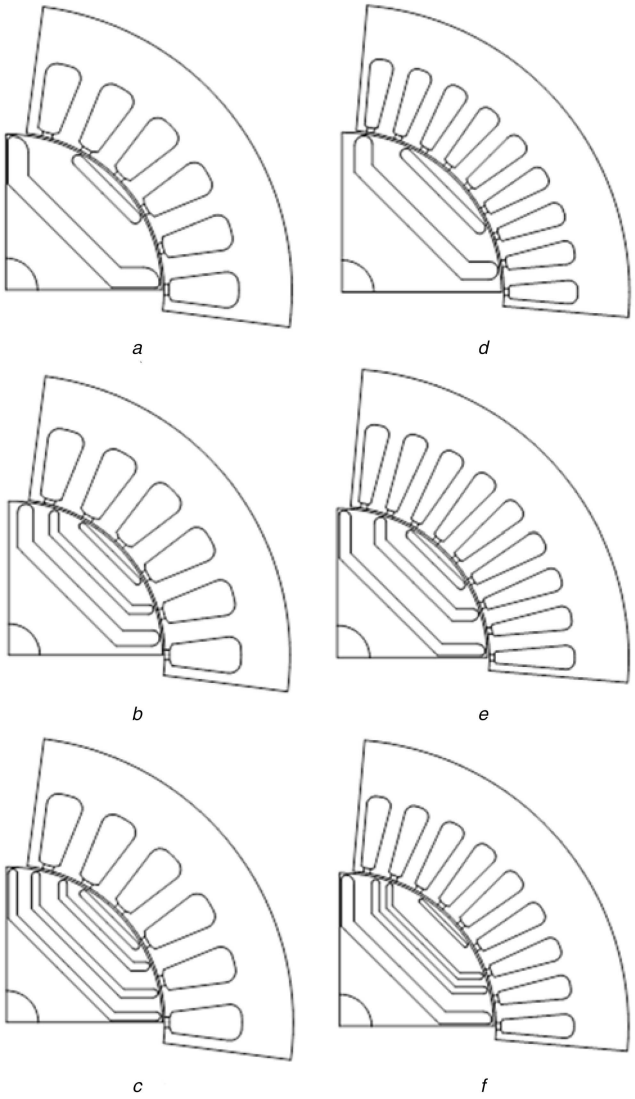

Fig. 4 *Machines selected after the T–ΔT optimisations at 1000 rpm:*
(a) *24 slots/2 barriers per pole,* ***(b)***, 24 slots/3 barriers per pole, ***(c)*** 24 slots/4 barriers per pole, ***(d)*** 36 slots/2 barriers per pole, ***(e)*** 36 slots/3 barriers per pole, ***(f)*** 36 slots/4 barriers per pole

Fig. 5 reports the electromagnetic torque, FEA evaluated, of the six machines for few significant values of the rotational speed. It can be noticed that as the speed increases, the average torque reduces due to the larger thickness of the radial ribs required to guarantee the rotor integrity. Moreover, for a given number of stator slots and total losses, the higher the number of barriers, the higher the torque. Lastly, the slots/barriers combinations which guarantee better performance in terms of average torque maximisation and torque ripple reduction are 24 slots/3 barriers per pole and 36 slots/4 barriers per pole. These results are consistent with those reported in the literature [6, 12, 23, 24]. Figs. 6 and 7 show the output power evaluated at different values of the mechanical speed for the considered machines; the rotor laminations corresponding to 30,000, 50,000, and 75,000 rpm are reported for sake of brevity. Fig. 6 refers to the machines with 24 stator slots; whereas Fig. 7 deals with machines with 36 slots.

Once again, all the machines share the same amount of admissible losses. When the mechanical speed increases, iron losses become higher because they are related to the electrical frequency; furthermore, the radial ribs become wider due to the increased centrifugal forces. Both these aspects reduce the torque capability of the SyR machines, as previously highlighted in Fig. 5.

From Figs. 6 and 7, two regions in the power-speed plane can be identified; therefore, a value of the rotational speed which maximises the output power, for a given value of admissible losses, can be found: below this speed value (first region), an increase in the rotational speed produces an increase in the output power; beyond this speed value (second region), the output power degrades because the reduction in the torque capability, due to the structural and thermal limitations, prevails over the speed increase. The speed which defines the border between the two regions, is about 60,000 rpm.

4 Output power–torque ripple optimisation

In this section, the second design procedure is described, namely the P–ΔT optimisation. Starting from the statements reported in Section 2, different cost functions for the DE optimisation are chosen: here, the first objective is the maximisation of the output power; the second one remains the minimisation of the torque ripple. Now, also, the mechanical speed is included among the optimisation parameters in order to automatically find the value of the rotational speed, which maximises the output power for a given amount of admissible losses. Therefore, each candidate machine is described by $2n_{\text{lay}} + 5$ parameters (where n_{lay} is the number of barriers per pole); the lower and upper bounds of the search space for the mechanical speed are set to 30,000 and 80,000 rpm, respectively. For the other optimised parameters, the search space is the same adopted for the T–ΔT optimisation.

Since the mechanical speed is varied during the optimisation, for each candidate machine the size of the rotor radial ribs is automatically adapted by means of the analytical model recalled in Section 2.3.

The output of each optimisation run is the Pareto front in the power–torque ripple plane. For sake of brevity, the results shown

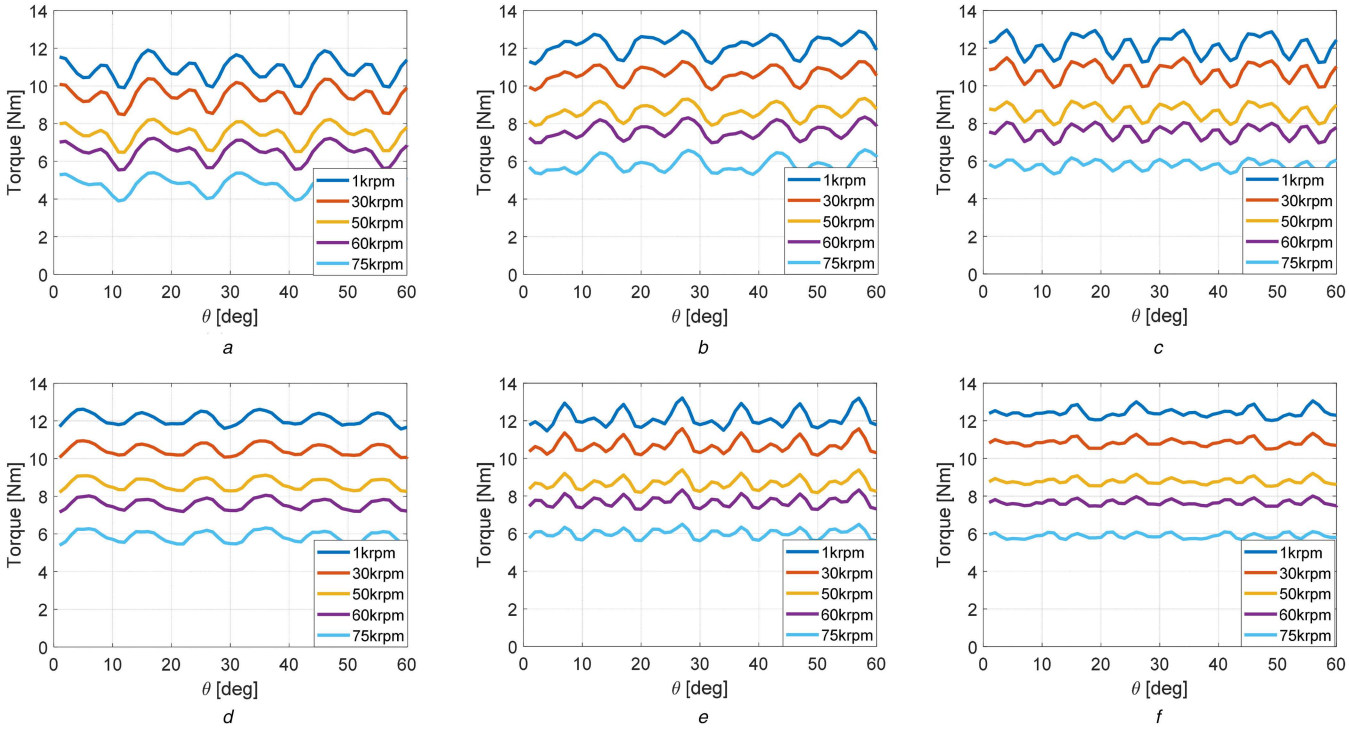

Fig. 5 *Torque versus rotor position for the machines selected after the T–ΔT optimisations at different rotational speeds*
(a) 24 slots/2 barriers, ***(b)*** 24 slots/3 barriers, ***(c)***, 24 slots/4 barriers, ***(d)*** 36 slots/2 barriers, ***(e)***, 36 slots/3 barriers, ***(f)*** 36 slots/4 barriers

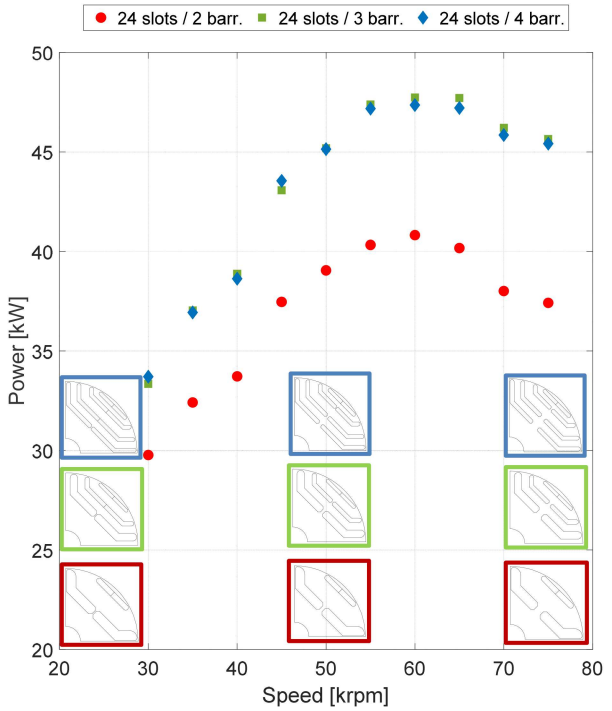

Fig. 6 *Output power versus rotational speed: machines with 24 slots and different numbers of barriers per pole*

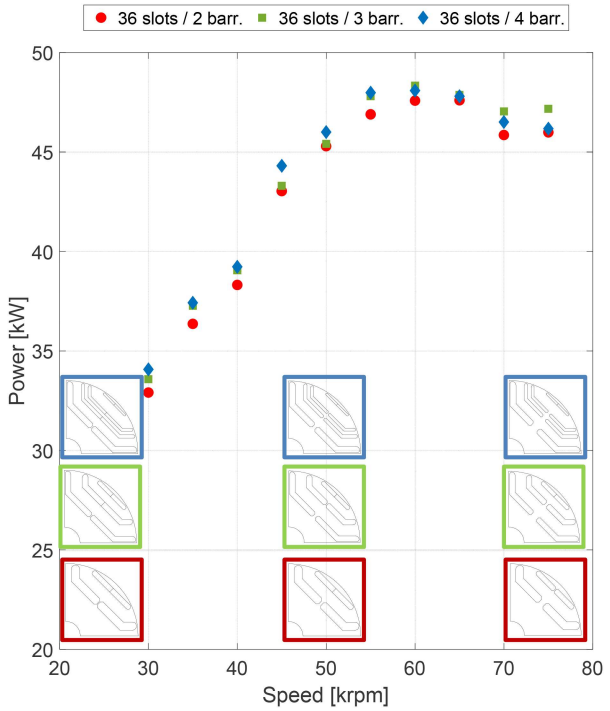

Fig. 7 *Output power versus rotational speed: machines with 36 slots and different numbers of barriers per pole*

below refer to the two slots/barriers combinations that seemed to be the most promising ones after the results shown in the previous section: 24 slots/3 barriers and 36 slots/4 barriers, hereafter referred to as 24/3 and 36/4 machines, respectively. Fig. 8 reports the Pareto fronts obtained after the P–ΔT optimisation and the selected machines, whereas Fig. 9 shows the evolution of the mechanical speed over the generations of the DE algorithm.

It can be noticed that the speed converges to a value of about 59,000 and 62,000 rpm for the 24/3 machine and the 36/4 machine, respectively; this can be considered the value above which no further improvement of the power capability can be obtained for the given mechanical and thermal constrains. Moreover, the convergence of the speed values proves the effectiveness of the proposed approach for the automated power maximisation. The sketches of one pole of the two aforementioned machines are shown in Fig. 10, whereas Table 4 reports their main performance figures.

5 Comparison between the design procedures

The two design procedures analysed in the previous sections aim at finding the maximum output power obtainable by a SyR machine, for fixed outer dimensions and admissible losses. The two procedures show similar outcomes: in both cases, the rotational speed, which maximises the output power, is about 60,000 rpm;

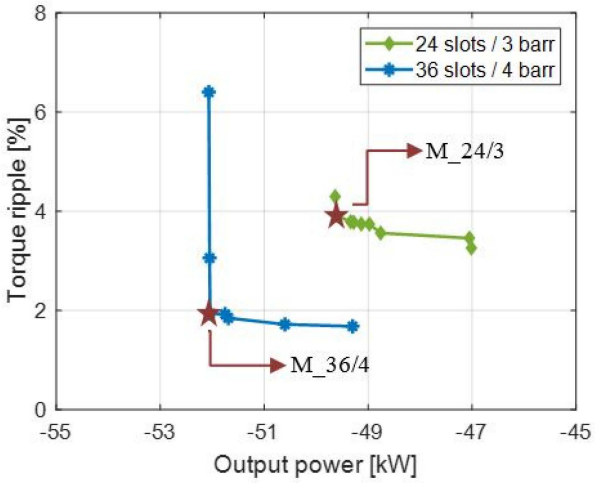

Fig. 8 *Pareto fronts obtained after the P–ΔT optimisations*

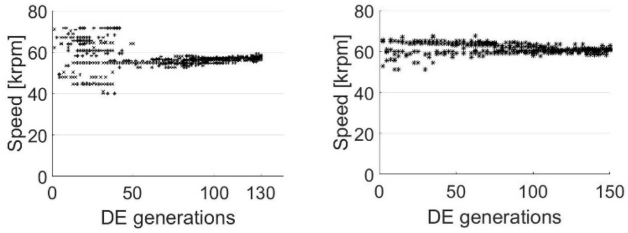

Fig. 9 *Evolution of the mechanical speed during the P–ΔT optimisations for the machines*
(a) 24/3, ***(b)*** 36/4

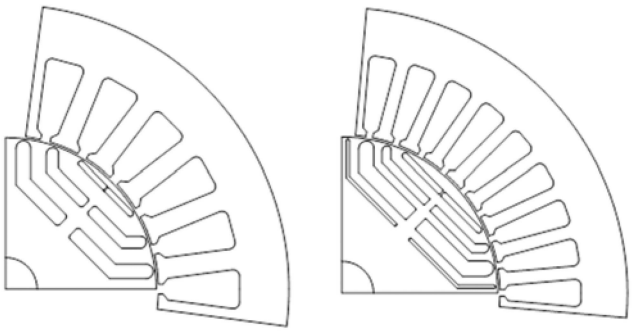

Fig. 10 *Machines selected after the P–ΔT optimisations:*
(a) M_24/3, ***(b)*** M_36/4

moreover, the optimal values of the split ratio and magnetic insulation ratio along the q-axis are similar (as evidenced by comparing Tables 3 and 4). Both procedures act on the entire geometry of the machine and can find non-conventional arrangements of the flux barriers, which cannot be predicted using the criteria suggested by the literature.

The T–ΔT procedure implies that a SyR machine optimally designed at low speed can be a good candidate also for high-speed applications provided that the rotor ribs are adapted to the actual speed. In other words, this procedure considers the electromagnetic problem and the structural one as weakly coupled. This assumption, which is not considered in the case of the P–ΔT optimisation, can lead to sub-optimal solutions.

The machines obtained after the P–ΔT procedure show a slightly higher power capability, for the same admissible losses: the output power improvement is about +4% for the 24/3 combination and +7.6% for the 36/4 one. Finally, it is worth noticing that, despite the increased computational burden required by a single optimisation run, the adoption of the proposed P–ΔT optimisation allows to find at the same time the maximum power obtainable from a SyR machine and the mechanical speed, which maximises

Table 4 Main performance figures of the optimal machines (P–ΔT optimisation)

Machine	Average torque, Nm	Torque ripple, Nm	Power factor	Saliency ratio (L_d/L_q)	Split ratio, %	Air to iron ratio, %
24 slots/3 barriers per pole	7.9	1.2	0.52	3.0	53	37
36 slots/4 barriers per pole	8.0	0.6	0.54	3.2	55	36

Table 5 Comparison between T–ΔT and P–ΔT optimisations

Machine 36 slots/4 barriers.	T–ΔT opt	P–ΔT opt
parameters varied by the optimisation algorithm	12	13
duration of the single optimisation run, h	12	14.5
max. speed automatically found by the algorithm	no	yes
maximum power, kW	48	52

Table 6 Parameters of the machine M_36/4 selected after the P–ΔT optimisation

Parameter	Value
stator tooth length, mm	12.80
stator tooth width, mm	2.11
stator inner radius, mm	24.56
barrier angle $\Delta\alpha_1$, deg.	20
barrier angle $\Delta\alpha_2$, deg.	7
barrier angle $\Delta\alpha_3$, deg.	8
barrier angle $\Delta\alpha_4$, deg.	7
barrier thickness h_{c1}, mm	1.0
barrier thickness h_{c2}, mm	1.4
barrier thickness h_{c3}, mm	2.4
barrier thickness h_{c4}, mm	0.5
mechanical speed, rpm	62,000
current angle γ, deg.	65

the output power. Therefore, dealing with the power density maximisation of SyR machines, the P–ΔT optimisation should be preferable. Table 5 resumes the comparison between the two procedures for the case of a SyR machine with 36 slots and 4 barriers per pole.

6 Accurate analysis of one SyR machine

One machine is selected from the P–ΔT Pareto front so as to perform an accurate electromagnetic and structural FEA aimed at evaluating the feasibility of a prototype and the validity of the proposed design approach. The results shown in the following regard the machine M_36/4 (highlighted in Fig. 8), whose optimization parameters are reported in Table 6

Fig. 11 shows the Von Mises stress distribution at 62,000 rpm evaluated on a refined version of the machine M_36/4. The radial ribs of the innermost barriers, obtained through the analytical model proposed in Section 2.3, are split into different parts in order to relax the stress; since the sum of the thicknesses of the radial ribs per each barrier is kept unchanged, this mechanical refinement does not influence significantly the electromagnetic behaviour of the machine [21]. The maximum stress is below 600 MPa, which is the yield strength of the lamination material; moreover, the maximum rotor displacement due to the centrifugal force is 30 μm.

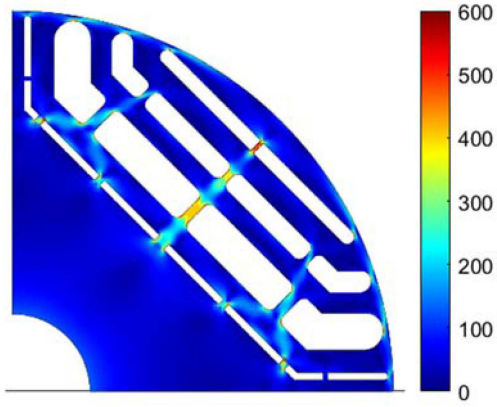

Fig. 11 *Von Mises stress distribution [MPa] at 62,000 rpm after the mechanical refinement M_36/4*

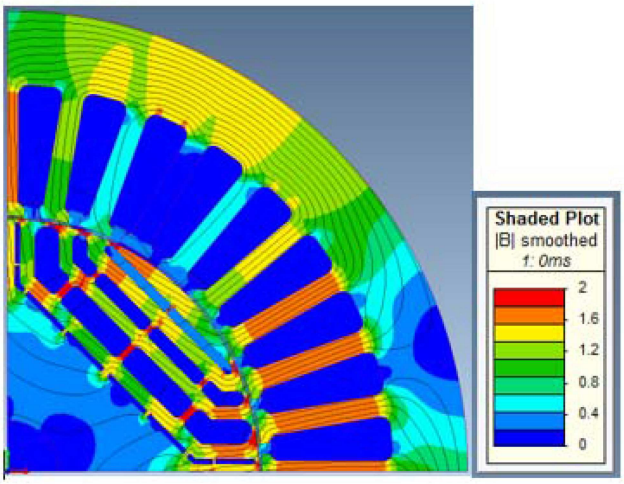

Fig. 12 *Flux density distribution at rated conditions*

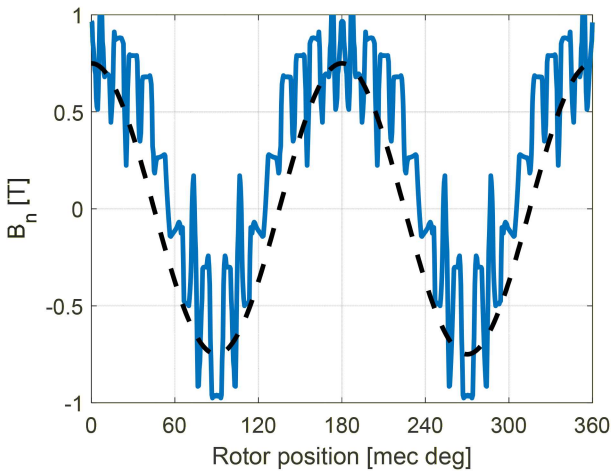

Fig. 13 *Normal component of the air gap flux density*

This confirms the suitability of the simplified model adopted for the sizing of the radial ribs during the optimisation stage.

The main results of the electromagnetic analysis performed through transient with motion FEA simulations considering 180 points over one electrical period, are presented in Figs. 12–14.

Fig. 12 shows the flux density distribution within one machine pole, whereas Fig. 13 reports the radial component of the air gap flux density over the entire air gap periphery, both evaluated at rated current along the MTPA. The peak value of the fundamental component of the flux density at the air gap (dashed line in Fig. 13) is about 0.7 T; the peak flux density in the stator teeth approaches 1.8 T (Fig. 12). Both figures testify the magnetic loading of rotor flux paths and stator teeth that are close to the knee of the magnetic characteristic of the silicon-iron alloy 10JNEX900 [18].

Fig. 14 reports the contours of average torque, power factor, and efficiency FEA evaluated considering a 15×15 mesh of equally spaced current points in the dq plane ranging from 0 to 1.5 times the rated current. The rated current loci are highlighted by dashed lines, whereas a dot represents the operating point at rated current and MTPA angle. The efficiency is between 97 and 98% in the operating region ranging from half load to full load along the MTPA trajectory. The power factor is quite low and approaches 0.55.

Finally, the machine M_36/4 obtained after the P–ΔT optimisation is compared with a 'conventional' SyR machine, referred to as C_36/4, designed following the guidelines proposed by the literature. The same stator lamination, air gap thickness, and admissible losses are considered for both machines. The rotor of C_36/4 is first designed considering a low speed, so as to neglect the radial ribs: its barriers are equally spaced at the air gap and their thickness is chosen so as to have constant permeance [6]. Then, the speed is increased up to 62,000 rpm and the radial ribs are sized so as to have the same stress levels as M_36/4.

Fig. 15 compares the torque profiles of the two machines and shows their rotor laminations. The proposed machine M_36/4 shows a slightly enhanced behaviour in terms of both average torque and torque ripple.

Table 7 summarises the main performance figures of the two machines, calculated at rated current and rated speed through transient-with-motion electromagnetic FEA. The total losses are 1 kW and are almost equally split between the windings and the iron laminations for the two machines; nevertheless, it is worth reminding that the rotor losses are <10% of the total power dissipated: this is an advantage considering that the heat produced by the rotor is more difficult to extract. The results reported in this section show the effectiveness of the proposed design procedure.

The main weakness of SyR machines remains the poor power factor, which would impact also on the sizing of the power converter coupled to the machine; this drawback is strictly related to the large thickness of the radial ribs required to ensure the rotor integrity at high-speed. The easiest way to overcome the power factor limitation can be the addition of PMs inside the flux barriers; however, the study of PM-assisted SyR machines is beyond the scope of this study and will be investigated in future works.

7 Conclusion

This study deals with the magnetic and mechanical co-design of SyR machines for high-speed applications. Two design procedures aimed at maximising the output power, for a given volume of active parts and admissible losses, were presented. Both procedures make use of optimisation algorithms in order to find non-conventional geometries which can be difficultly predicted through standard analytical models. Different slots/barriers combinations were analysed and compared, showing their influence on the power density maximisation.

The P–ΔT optimisation procedure, even though more expensive from a computational standpoint, led to machines with slightly higher output power; moreover, it allowed to find, at the same time, the power limit and the rotational speed, which maximises the power density of a SyR machine for given thermal and structural constraints.

8 Acknowledgments

This work was supported in part by the project WindMill 4.0, code N7P89U5 – INNONETWORK 2017, POR Puglia FESR- FSE 2014–2020.

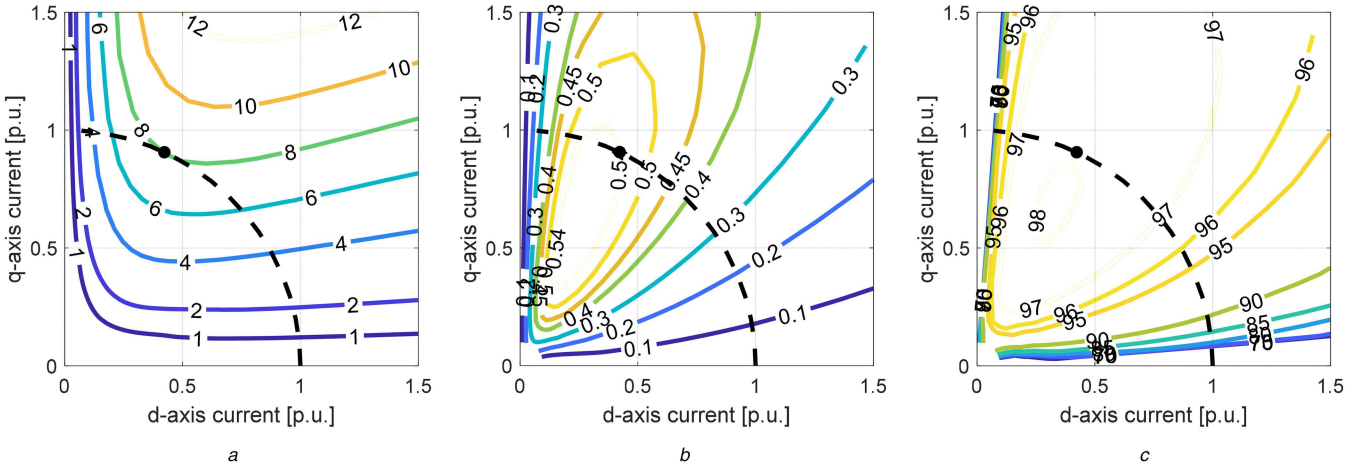

Fig. 14 *Contour plots of*
(a) *Average torque,* ***(b)*** *Power factor* ***(c)****, Efficiency in the dq-plane for the machine M_36/4*

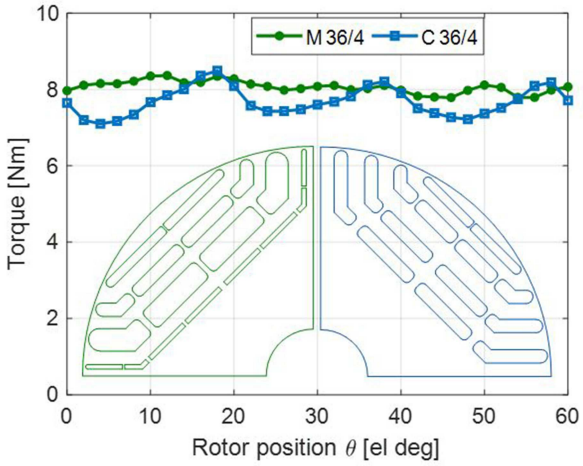

Fig. 15 *Comparison between M_36/4 and C_36/4*

Table 7 Comparison between a conventional machine (C_36/4) and the output of the *P*–Δ*T* optimisation (M_36/4)

Parameter	M_36/4	C_36/4
output power, kW	52	50
rotational speed, krpm	62	62
rotor tip speed, m/s	157	157
torque ripple, Nm	0.6	1.4
saliency ratio	3.2	3.0
copper loss, W	530	525
iron loss (stator), W	403	407
iron loss (rotor), W	84	88
power factor	0.54	0.51

9 References

[1] Pellegrino, G., Jahns, T. M., Bianchi, N., *et al.*: '*The rediscovery of synchronous reluctance and ferrite permanent magnet motors*' (Springer International Publishing, Switzerland, 2016)

[2] Palmieri, M., Perta, M., Cupertino, F.: 'Design of a 50.000-rpm synchronous reluctance machine for an aeronautic diesel engine compressor', *IEEE Trans. Ind. Appl.*, 2016, **52**, (5), pp. 3831–3838

[3] Howard, E., Kamper, M. J.: 'Reluctance synchronous wind generator design optimisation in the megawatt, medium speed range'. Proc. 2017 IEEE Energy Conversion Congress and Exposition (ECCE), Cincinnati, OH, September 2017, pp. 1864–1871

[4] Kärkkäinen, H., Aarniovuori, L., Niemelä, M., *et al.*: 'Technology comparison of induction motor and synchronous reluctance motor'. Proc. 43rd Annual Conf. of the IEEE Industrial Electronics Society, Beijing, China, October 2017, pp. 2207–2212

[5] Babetto, C., Bacco, G., Bianchi, N.: 'Design methodology for high-speed synchronous reluctance machines', *IET Electr. Power Appl.*, 2018, **12**, (8), pp. 1110–1116

[6] Vagati, A., Pastorelli, M., Francheschini, G., *et al.*: 'Design of low-torque-ripple synchronous reluctance motors', *IEEE Trans. Ind. Appl.*, 1998, **34**, (4), pp. 758–765

[7] Moghaddam, R., Gyllensten, F.: 'Novel high-performance SynRM design method: an easy approach for a complicated rotor topology', *IEEE Trans. Ind. Electron.*, 2014, **61**, (9), pp. 5058–5065

[8] Babetto, C., Bianchi, N., López, C., *et al.*: 'High-speed synchronous reluctance motors: computation of the power limits by means of reluctance networks'. Proc. IEEE 18th Int. Power Electronics and Motion Control Conf. (PEMC), Budapest, Hungary, August 2018, pp. 556–561

[9] Di Nardo, M., Galea, M., Gerada, C., *et al.* F.: 'Multi-physics optimization strategies for high speed synchronous reluctance machines'. Proc. 2015 IEEE Energy Conversion Congress and Exposition (ECCE), Montreal, QC, September 2015, pp. 2813–2820

[10] Bramerdorfer, G., Tapia, J. A., Pyrhönen, J. J., *et al.*: 'Modern electrical machine design optimization: techniques, trends, and best practices', *IEEE Trans. Ind. Electron.*, 2018, **65**, (10), pp. 7672–7684

[11] Cupertino, F., Pellegrino, G., Gerada, C.: 'Design of synchronous reluctance motors with multiobjective optimization algorithms', *IEEE Trans. Ind. Appl.*, 2014, **50**, (6), pp. 3617–3627

[12] Palmieri, M., Perta, M., Cupertino, F., *et al.*: 'Effect of the numbers of slots and barriers on the optimal design of synchronous reluctance machines', *J. Elect. Eng.*, 2015, **15**, (1), pp. 325–333

[13] Howard, E., Kamper, M. J., Gerber, S.: 'Asymmetric flux barrier and skew design optimization of reluctance synchronous machines', *IEEE Trans. Ind. Appl.*, 2015, **51**, (5), pp. 3751–3760
[14] Kiani, M., Bostanci, E., Fahimi, B.: 'Optimal design of synchronous reluctance machines'. Proc. 43rd Annual Conf. of the IEEE Industrial Electronics Society, Beijing, China, October 2017, pp. 3749–3753
[15] Cupertino, F., Leuzzi, R., Monopoli, V. G., *et al.*: 'Maximisation of power density in permanent magnet machines with the aid of optimisation algorithms', *IET Electr. Power Appl.*, 2018, **12**, (8), pp. 1067–1074
[16] Cupertino, F., Palmieri, M., Pellegrino, G.: 'Design of high-speed synchronous reluctance machines'. Proc. 2015 IEEE Energy Conversion Congress and Exposition (ECCE), Montreal, QC, September 2015, pp. 4828–4834
[17] Syre. Available at http://sourceforge.net/projects/syr-e/
[18] 10JNEX900. Available at http://www.jfe-steel.co.jp/en/
[19] Price, K. V., Storn, R. M., Lampinen, J. A.: '*Differential evolution-a practical approach to global optimization*' (Springer-Verlag, Switzerland, 2005)
[20] Wang, Y., Ionel, D. M., Rallabandi, V., *et al.*: 'Large-scale optimization of synchronous reluctance machines using CE-FEA and differential evolution', *IEEE Trans. Ind. Appl.*, 2016, **52**, (6), pp. 4699–4709
[21] Palmieri, M., Cupertino, F., Cascella, G. L.: 'Mechanical refinements for the stress reduction of high-speed synchronous reluctance machines'. Proc. 2018 XIII Int. Conf. on Electrical Machines (ICEM), Alexandroupoli, Greece, 2018, pp. 826–832
[22] Diao, X., Zhu, H., Qin, Y., *et al.*: 'Torque ripple minimization for bearingless synchronous reluctance motor', *IEEE Trans. Appl. Supercond.*, 2018, **28**, (3), pp. 1–5
[23] Howard, E., Kamper, M. J.: 'Weighted factor multiobjective design optimization of a reluctance synchronous machine', *IEEE Trans. Ind. Appl.*, 2016, **52**, (3), pp. 2269–2279
[24] Tap, A., Xheladini, L., Asan, T., *et al.*: 'Effects of the rotor design parameters on the torque production of a PMaSynRM for washing machine applications'. Proc. 2017 Int. Conf. on Optimization of Electrical and Electronic Equipment (OPTIM) & 2017 Intl Aegean Conf. on Electrical Machines and Power Electronics (ACEMP), Brasov, 2017, pp. 370–375